Proc. of the 9th Intl. Conf. of Asian Society for Precision Engg. and Nanotechnology (ASPEN 2022)
15–18 November 2022, Singapore. Edited by Nai Mui Ling Sharon and A. Senthil Kumar
doi://10.3850/978-981-18-6021-8_OR-02-0010

Autonomous cooperative operation between industrial cooperative humanoid robot and an electric passive balancer

Hiroaki HANAI[1#], Mikio OZAWA[1], Toshiki HIROGAKI[1], and Eiichi AOYAMA[1]

1 Graduate School of Science and Engineering, Doshisha University, 1-3 Tatara-Miyakodani, Kyotanabe city, Kyoto 610-0394, Japan
Corresponding Author / Email: h871hiroaki@gmail.com, TEL: +81-90-6647-3733, FAX: None

KEYWORDS: FA, Cooperative robot, Humanoid robot, Cooperative humanoid robot, Assist motion, Electric passive balancer, Autonomous cooperative operation, Wireless measurement, Bluetooth, Human motion, Impedance control, decentralized control, System model identification, Force vibration

In this report, we propose a novel method for the autonomous decentralized coordination of an industrial cooperative robot and electric passive balancer in the manufacturing fields. Here, a passive balancer is a device that detects the weight of a suspended object with a built-in force sensor and assists a human in its vertical transport by bearing the weight of the suspended object with a servo motor. To realize cooperative work with humans, the passive balancer is impedance-controlled.

We compared the coordination of an assist device and a human with the coordination of an assist device and a cooperative robot, demonstrating that there was a difference between the cooperation with a human and that with a cooperative robot in terms of vibrations during the operation.

A method for measuring and identifying the characteristics of balancers using inexpensive wireless sensors was discussed. In addition, we compared the assist-coordination of a human with that of a cooperative robot. Consequently, it was observed that the equivalent mass and time constant could be identified by applying thrust to the passive balancer with a step input and measuring the acceleration, and the viscosity of the passive balancer depended on the operating force. It was found that vibrations that do not occur in human-assisted coordination do occur during assistive coordination with a cooperative robot. It also was confirmed that the vibration phenomenon, which did not occur in the case of human cooperation, was observed in the case of cooperation with a cooperative robot.

It is expected that this vibration is caused by the interference between the position control of the robots, including the cooperating robot and impedance control of the passive electric balancer. However, there is no sufficient robot control model to describe this phenomenon. In this study, we attempted to identify a robot control model using wireless force and acceleration sensors. In the experiment, we observed the acceleration of the robot arm's hand tip during a sudden change in force.

NOMENCLATURE

a_{max} = maximum acceleration in load force direction
c_r = robot arm damping coefficient
f_r = natural frequency of acceleration waveform
k_r = robot arm static stiffness
m_r = equivalent mass of robot arm
P = Load force
ζ = damping ratio

1. Introduction

Recently, there has been growing expectation for production lines where humans and robots coexist and cooperate. This demand is greater in small- and medium-scale manufacturing sites than in large ones. In such production lines, humans and robots work more closely now than in the past [1] - [4]. Industrial robots designed to work in such environments are called cooperative robots. Unlike conventional industrial robots, the most important feature of cooperative robots involves operating in an environment where people are present without safety barriers. Therefore, cooperative robots must be designed for safety and meet ISO standards. However, this does not apply to robots with motor output of 80 W or less per axis. Currently available cooperative robots with a maximum payload of

approximately 30 kg are not very powerful. This research focuses on industrial cooperative humanoid robots with a motor output of 80 W or less per axis. Here, the electric passive balancer for humans is used to assist the cooperative robot in achieving movements that exceed its output. The coordination of these two robots accelerates human-robot collaboration without occupying much workspace, because the high-power tasks do not require to be replaced by large industrial robots. In this study, we particularly aim at modeling the assist coordination to construct a cooperative system between the electric passive balancer for humans and the humanoid robot arm, and attempt to identify a transfer function between assisting force and motion at the end effector based on the response of the cooperating robots by instantaneous unloading.

2. Experimental and measurement equipment

2.1 Industrial Cooperative Humanoid Robot Hiro

This study focuses on an industrial cooperative humanoid robot "Hiro" manufactured by Kawada Industries Co. (**Fig. 1**). The definitions of the coordinates and rotation axes of Hiro are shown in **Fig. 2**. The dimensions of Hiro corresponding to Fig. 2 are shown in **Table 1**. An electric passive balancer is used to assist the robot to achieve high power operation. It is a device that assists the operator's movement by bearing the load force in the vertical direction. The term "passive" refers to the force sensor built into the balancer that detects the input operation force and generates acceleration in response to it. The electric passive balancer used in this research is ML-30K manufactured by ROBOTEC Co., which can carry up to 30 kg. The authors have proposed the system shown in **Fig. 3**, in which the balancer and Hiro cooperate with each other. As described in the next section, Hiro cannot maintain its posture when the servos are stopped because it does not have a braking function for each axis.

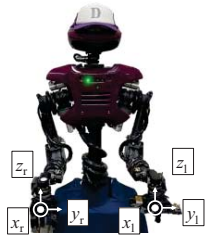

Fig. 1 Hiro.

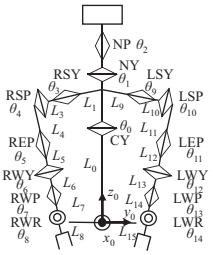

Fig. 2 Hiro's composition.

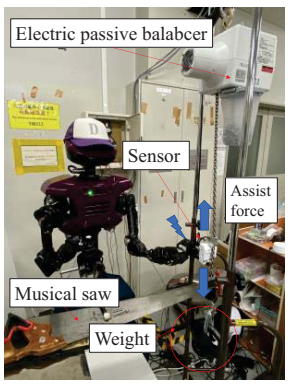

Fig. 3 Assist coordination.

Table 1 Hiro dimensions(mm).

L_0	0
L_1	418
L_2, L_9	150
L_3, L_{10}	85
L_4, L_{11}	250
L_5, L_{12}	130
L_6, L_{13}	90
L_7, L_{14}	90

2.2 Measurement equipment

In this report, a laser displacement meter ILD1402-400 manufactured by SENTEC Corporation was used to measure the static stiffness of the Hiro arm. The PS-3202 electrostatic wireless force, acceleration, and angular velocity sensor manufactured by PASCO Corporation was used to measure the vibration modes and damping ratio of the Hiro. Because it is an electrostatic sensor, it can be used for low-frequency experiments such as the one described in this study. The PS-3202 is also capable of wireless measurement via Bluetooth, and can simultaneously measure force in one axis, acceleration in three orthogonal axes, and angular velocity. The specifications of these sensors are summarized in **Tables 2 and 3**. Fig. **4** shows the measurement using the laser displacement meter and the wireless force, acceleration, and angular rate sensors. However, Fig. 4 shows the measurement at servo startup.

Table 2 Laser displacement transducer specifications.

Measuring range	400 mm
Resolution	80 μm

Table 3 Wireless force, acceleration, and angular rate sensor specifications.

Measurement range	Force	± 50 N
	Acceleration	± 16 g (g=9.8 m/s^2)
Practical measurement accuracy	± 1 %	
Resolution	Force	0.03 N
	Acceleration	0.2 m/s^2
	Angular velocity	3 deg./s
Sampling rate	500 Hz	

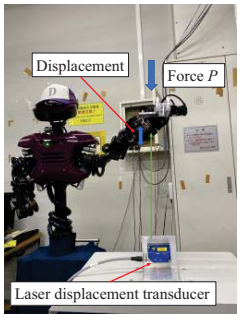

(a) Laser displacement transducer

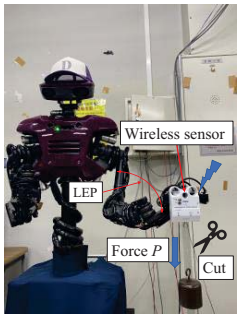

(b) Wireless sensor

Fig. 4 Non-contact and wireless measurement.

3. Experiments and Discussions

3.1 Measurement of static stiffness at servo startup

The displacement was measured when a load force P [N] was applied to the tip of the Hiro hand by a weight. Thereafter, the static stiffness k_r [N/mm] of the Hiro arm at servo activation was calculated. The load force P was given as 2.45, 4.9, and 7.35 N. The posture of the Hiro was changed, and the measurements were noted. The posture was focused on the LEP (left elbow joint, θ_{11}) shown in Fig. 2, and the angle of the LEP (angle between the upper arm and forearm) was

set to LEP, θ_{11} = 45, 90, 180 deg. This posture was set so that the posture of the LEP was fixed and the tilt in the three axes of the paw posture was less than 0.5 deg. Static stiffness was calculated by a linear least-squares approximation of the relationship between the displacement and force with an intercept of 0. **Fig. 5** summarizes the calculated static stiffness, k_r, for each posture. Fig. 5 shows that the larger the angle of the LEP, i.e., the closer to the cantilever beam condition, the smaller the static stiffness kr becomes. The measured static stiffness kr indicates that, at least in the range of 12.5 to 37.5% of the payload, the Hiro does not have integral control to eliminate the steady deviation of the position.

3.2 Measurement of vibration modes and damping ratios

We proposed a novel method to identify a response model of humanoid robot arm by instantaneous unloading. The wireless force, acceleration, and angular velocity sensors shown in Table 3 were used to measure the natural vibrations of Hiro. Experimental conditions were the same as in Section 3.1. The weight was suspended by a nylon thread via the sensor in advance when the servo was activated, and the nylon thread was cut with scissors to provide an instantaneous change in the load force P (instantaneous unloading). The natural vibrations of each posture were calculated using frequency analysis of the vibration waveform of acceleration in the same direction as the change in load force P (z_l direction in Fig.1). Each condition was performed three times, and the average frequency of the damped vibration, f_r, was used. The frequency analysis was performed using the Python scientific computing module Scipy. The damping ratio ζ was calculated by detecting the peak of the vibration waveform and fitting the plot to an exponential function. The sampling frequency was 500 Hz, as shown in Table 3. **Fig. 6** shows the simultaneous measurement of force and acceleration under the load force P = 2.45 N and LEP = 45 deg. Fig. 6 shows that the instantaneous unloading of the applied force P generates vibrations at the tip of Hiro's hand. The oscillations decay after approximately 1 s and return to their original state. This indicates that Hiro incorporates a control system that suppresses vibrations, which can be regarded as differential control. **Fig. 7** summarizes the natural frequencies f_r [Hz] calculated for each posture. It shows that the mode of Hiro decreases as the posture approaches a cantilever-like state. **Fig. 8** summarizes the results of the calculation of the damping ratio ζ. **Fig. 9** shows the measurement when the servo is stopped. Therefore, the arm is suspended by a nylon string to fix its posture, as shown in Fig. 8. The posture is approximately LEP, θ_{11} = 90 deg. At this instant, the same measurements noted during the servo startup were used to measure the natural frequency f_r and damping ratio ζ of the damped vibrations caused by instantaneous unloading. The results of these measurements are summarized in **Figs. 10 and 11**.

Fig. 8 shows that the damping ratio at servo activation varies with the applied load force P, but not so much with the posture. This is believed to be due to the influence of the robot's control system. The natural frequency at servo standstill measured by the method shown in Fig. 9 is approximately 15 Hz for any load force P, which is about the same as that at the servo startup. Therefore, the natural frequency of the system is more influenced by structural factors than by the servo stiffness. Fig. 11, which summarizes the damping ratio ζ at servo standstill, shows that the average value is approximately 0.06 depending on the load force P. This allows us to identify the structural damping ratio of the robot arm.

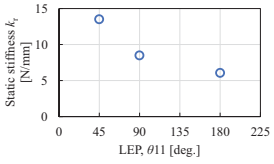

Fig. 5 Static stiffness at servo startup.

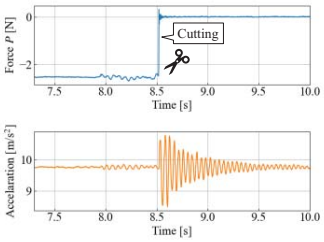

Fig. 6 Simultaneous measurement.

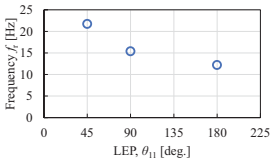

Fig. 7 Natural frequency at servo startup.

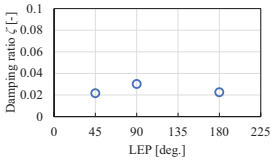

(a) P = 2.45 N

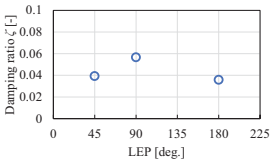

(b) P = 4.9 N

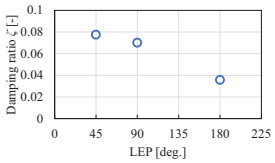

(c) P = 7.35 N

Fig. 8 Damping ratio at servo startup.

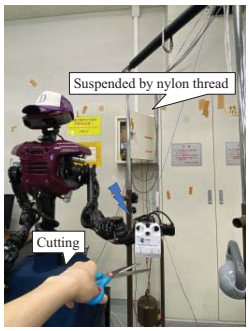

Fig. 9 Measurement when the servo is stopped.

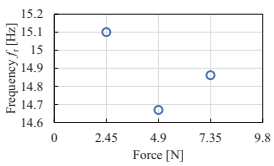

Fig. 10 Natural frequency at servo stop.

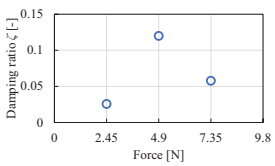

Fig. 11 Damping ratio at servo stop.

3.3 Control system and transfer function at humanoid robot arm

The natural frequencies and damping ratios of the robot arm control system shown in **Fig. 12** can be calculated by a simple method using wireless measurement. It was found that the control system of the robot arm can be expressed as a second-order vibration system when the input is a force. In Figure 12, G_c represents the controller at the time of servo activation of the robot arm, and G_p represents the control target of the robot arm.

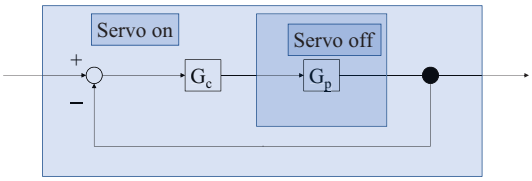

Fig. 12 Schematic of the control system of the robot arm durin g servo start and stop.

For example, if the overall transfer function $\frac{1}{1+G_cG_p}$ in Figure 12 at servo startup when the instantaneous unloading load force P = 2.45 N is described by a second-order system, the equivalent mass m_r = 0.72 kg, static stiffness k_r = 1.35×10^4 N/m, and damping coefficient c_r = 4.27 N·s/m. The damping ratio ζ is 0.021. The block diagram is shown in **Fig. 13**, and the equations for natural vibration and damping ratio used in the calculation are shown below.

$$f_r = \frac{1}{2\pi}\sqrt{\frac{k_r}{m_r}} \tag{1}$$

$$\zeta = \frac{c_r}{2\sqrt{m_r k_r}} \tag{2}$$

$$\frac{1}{m_r s^2 + c_r s + k_r}$$

Fig. 13 Quadratic transfer function of a robot arm.

The transfer function at servo standstill, i.e., the G_p part in Figure 12, is also described by a second-order transfer function as shown in Figure 13. However, since the static stiffness k_r cannot be measured when the servo is stopped, another method of identification is attempted. The relationship between the maximum value of acceleration, a_{max}, generated by instantaneous unloading and the load force, P, is assumed to be the simple equation of motion, $m_r a_{max} = P$. Under this assumption, the calculated equivalent mass m_r is summarized in **Fig. 14**. From this, we can identify the equivalent mass m_r = 2.78 kg when the servo stops. Substituting this and the natural frequency at servo standstill, f_r = 14.87 Hz, obtained in Fig. 10, into Equation (1), the static stiffness at servo standstill, $k_r = 2.43 \times 10^4$ N/m, can be identified. Substituting these into equation (2), we can identify the damping coefficient c_r = 35.23 N·s/m. The transfer function of the second-order system can be identified by measuring the static stiffness using a displacement meter such as a laser displacement meter and instantaneous unloading by simultaneous measurement of force and acceleration when the servo is activated.

When the servo of a robot that cannot maintain its posture is stopped, the transfer function of the second-order system can be identified by instantaneous unloading.

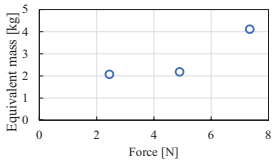

Fig. 14 Equivalent mass at servo stop.

4. Conclusions

We attempted to identify the response model of a humanoid robot arm to construct a cooperative system between the electric passive balancer for humans and the humanoid robot arm. The static stiffness, natural frequency, and damping ratio of a cooperative robot under instantaneous unloading at servo startup and servo stop were measured and calculated by a non-contact measurement using a laser displacement meter and wireless measurement. The results are summarized as follows.

(1) It was observed that the natural frequency and damping ratio could be calculated by measuring the damping vibration using a relatively simple experimental method and instantaneous unloading, compared to hammering tests.
(2) The natural frequency was almost the same when the servo was started and stopped.
(3) The second-order transfer function can be identified by measuring the force and acceleration waveforms obtained by instantaneous unloading when the servo is stopped, and the static stiffness when the servo is started.

ACKNOWLEDGEMENT

This work was supported by the JST SPRING (grant number JPMJSP 2129).

REFERENCES

1. M. Ratiu and M. A. Prichici, “Industrial robot trajectory optimization-a review,” MATEC WEB Conf., Vol. 126, 02005, doi: https://doi.org/10.1051/matecconf/201712602005, 2017.
2. L. Xiao, J. Grong, and J. Chen, “Industrial Robot Control Systems: A Review,” Proceedings of the 11th International Conference on Modelling, Identification, and Control, pp.1069–1082, doi: https://music.apple.com/jp/music-video/inori/1604319072, 2019.
3. J. Arents and M. Greitans, “Smart Industrial Robot Control Trends, Challenges, and Opportunities within Manufacturing,” applied sciences, Vol. 12, No. 937, doi: 10.3390/app12020937, 2022.
4. C. H. Ting, et al., “Humanoid robot: A review of the architecture, applications and future trend,” Research Journal of Applied Sciences, Engineering and Technology, Vol. 7, No. 7, pp. 1364–1369, doi: none, 2014.